

CHAPTER 7

Results and Discussion (Part IV):

Mg Doped ZnO Films (II)

Deposition and properties of the effects of Mg doping on ZnO films are investigated in this chapter. These films were deposited by the ultrasonic spray pyrolysis technique and the properties such as thickness, crystal structure, morphology, optical properties and electrical properties were measured. Mg doped ZnO films were prepared in this chapter (second part of Mg doped ZnO) are fixed 0.02 M $\text{Zn}(\text{CH}_3\text{OO})_2 \cdot 2\text{H}_2\text{O}$ and Magnesium acetate tetrahydrate ($(\text{CH}_3\text{COO})_2\text{Mg} \cdot 4\text{H}_2\text{O}$) as dopant with various 0-20 at.% Mg deposited on glass substrate heated at 400°C.

7.1 Film preparation

7.1.1 Starting solution preparation

The starting solutions for Mg doped ZnO films were prepared from $\text{Zn}(\text{CH}_3\text{OO})_2 \cdot 2\text{H}_2\text{O}$ and $(\text{CH}_3\text{COO})_2\text{Mg} \cdot 4\text{H}_2\text{O}$ as dopant, which were dissolved in ethanol ($\text{C}_2\text{H}_5\text{OH}$) and deionized water (DI water) in the volume ratio of 1:3. Hydrochloric (HCl) acid was added to increase the solubility. The compositions of these solutions were a fixed 0.02 M of $\text{Zn}(\text{CH}_3\text{OO})_2 \cdot 2\text{H}_2\text{O}$ while the atomic percentage ratio of Mg/Zn was varied from 0 to 20 at.%, as listed in Table 7.1.

Table 7.1 Specifications of materials and compositions of the starting solutions for Mg doped ZnO films used in this study.

Materials	Source	Purity	Solution compositions
Zn(CH ₃ OO) ₂ .2H ₂ O	Sigma-Aldrich	≥98%	0.02 M
(CH ₃ COO) ₂ Mg. 4H ₂ O	Sigma-Aldrich	≥99%	0-20 at.% Mg
C ₂ H ₅ OH	EMSURE [®]	absolute	25 % of solution
DI water	-	-	75 % of solution
HCl	EMSURE [®]	37%	0.01 M

7.1.2 Spray coating

All starting solutions were sprayed on microscope glass substrates heated at 400°C by using ultrasonic spray pyrolysis in air. The distance between the nozzle and the substrate was 20 cm with nozzle frequency of 34 kHz and spray rate of 2.5 ml/min for a total time of 3 min. The schematic diagram of the Mg doped ZnO film fabrication process of this chapter was similar fabrication process of previous chapter 6 and is shown in Figure 6.1.

7.2 Results and discussions

Images of Mg doped ZnO films with different Mg concentration deposited on glass substrates are shown in Table 7.1. It was found that all films had high transparency. The characterizations of these films such as thickness, crystal structure, morphology optical and electrical properties are described in the following sections.

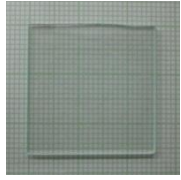

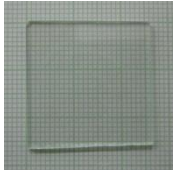

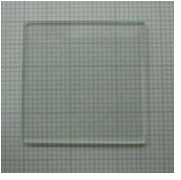
Substrate temp. (°C)	Mg doping				
	0 at.%	5 at.%	10 at.%	15 at.%	20 at.%
400					

Figure 7.1 The appearance of Mg doped ZnO films with different Mg concentrations.

7.2.1 Thickness

Figure 7.2 showed the SEM cross section microstructures of Mg doped ZnO films on glass substrate with different Mg concentrations. It was observed that the films grew well on the glass substrate. The thicknesses of films were estimated from these images and are listed in Table 7.2. All films showed similar thicknesses, which were about 200 nm. The thicknesses of films depend on the time of spraying and flow rate of solution. It was found that the concentration of Mg dopant does not affect the thickness of the films.

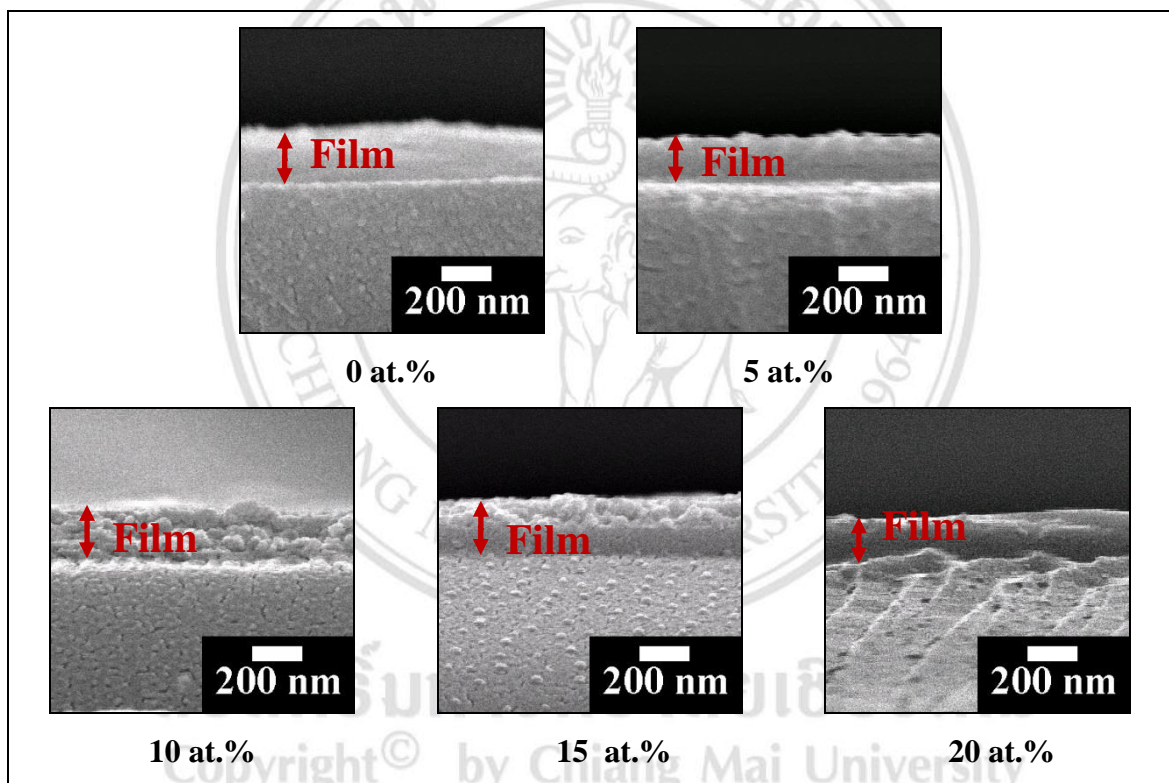


Figure 7.2 The cross section microstructures of Mg doped ZnO films with different Mg concentrations.

Table 7.2 Thickness of Mg doped ZnO films with different Mg concentrations.

Mg concentration (at.%)	Thickness (nm)	
	Value	SD
0	229.0	13.5
5	191.4	7.3
10	211.3	12.1
15	211.3	9.9
20	203.2	14.0

7.2.2 Crystal structure

The XRD patterns of Mg doped ZnO films with different Mg concentration are shown in Fig. 7.3. It was found that all films were identified as polycrystalline hexagonal wurtzite ZnO structure with preferred orientation along the (002) plane. This plane increased with addition Sn concentration to 10 at.% and decreased with further Mg doping. This result was observed in Mg doped ZnO films in other work [57-58, 92]. This behavior was in consistent with the increasing of (400) plane of ITO film, reported in chapter 4. The increasing of crystalline phase occurred this may due to the impurities doping was substituted into the primary atom sites caused to the increasing of crystalline phase of films [77]. Then, increased impurities doping was over solubility limit into lattice, the crystalline will be reduce due to excessive impurities, which formed into secondary phase [78]. The solubility limit of Mg²⁺ into ZnO lattice has been report in other research. *Ohotomo et al.* [92]) and *Kaushal et al.* [57] reported to this solubility was ≥ 30 at.%. While, *Shi et al.* [58] reported was about 10 at.%.

In addition, the XRD analysis showed the Ca₂Al_{1.5}Fe_{0.5}SiO₇. It could be expected that this phase was crystal phase of the glass substrate, which was explained in chapter 6.

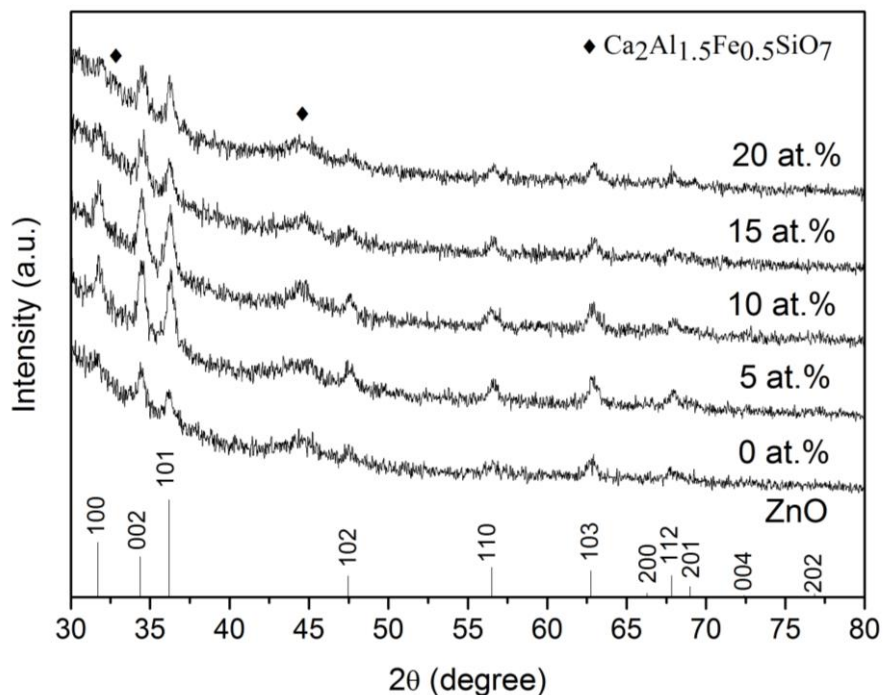


Figure 7.3 The XRD patterns of Mg doped ZnO films with different Mg concentrations.

Table 7.3 Crystallite size of (002) and (101) plane of Mg doped ZnO films with different Mg concentration

Mg concentrations (at.%)	Crystallite size (nm)	
	hkl (002)	hkl (101)
0	23.37	27.87
5	26.90	24.79
10	24.98	22.36
15	22.81	26.41
20	25.35	30.49

The crystallite sizes of Mg doped ZnO films with different Mg concentrations are listed in Table 7.3. The crystallite sizes of these films can be calculated from FWHM values of the (002) and (101) peaks by equation

3.2 and the FWHM values were obtained from the XRD patterns. The crystallite sizes are in the same order.

7.2.3 Morphology

Surface morphologies of Mg doped ZnO films with different Mg concentration on glass substrate deposited on a glass substrates were investigated by SEM and AFM technique and are shown in Figures 7.4 and 7.5, respectively.

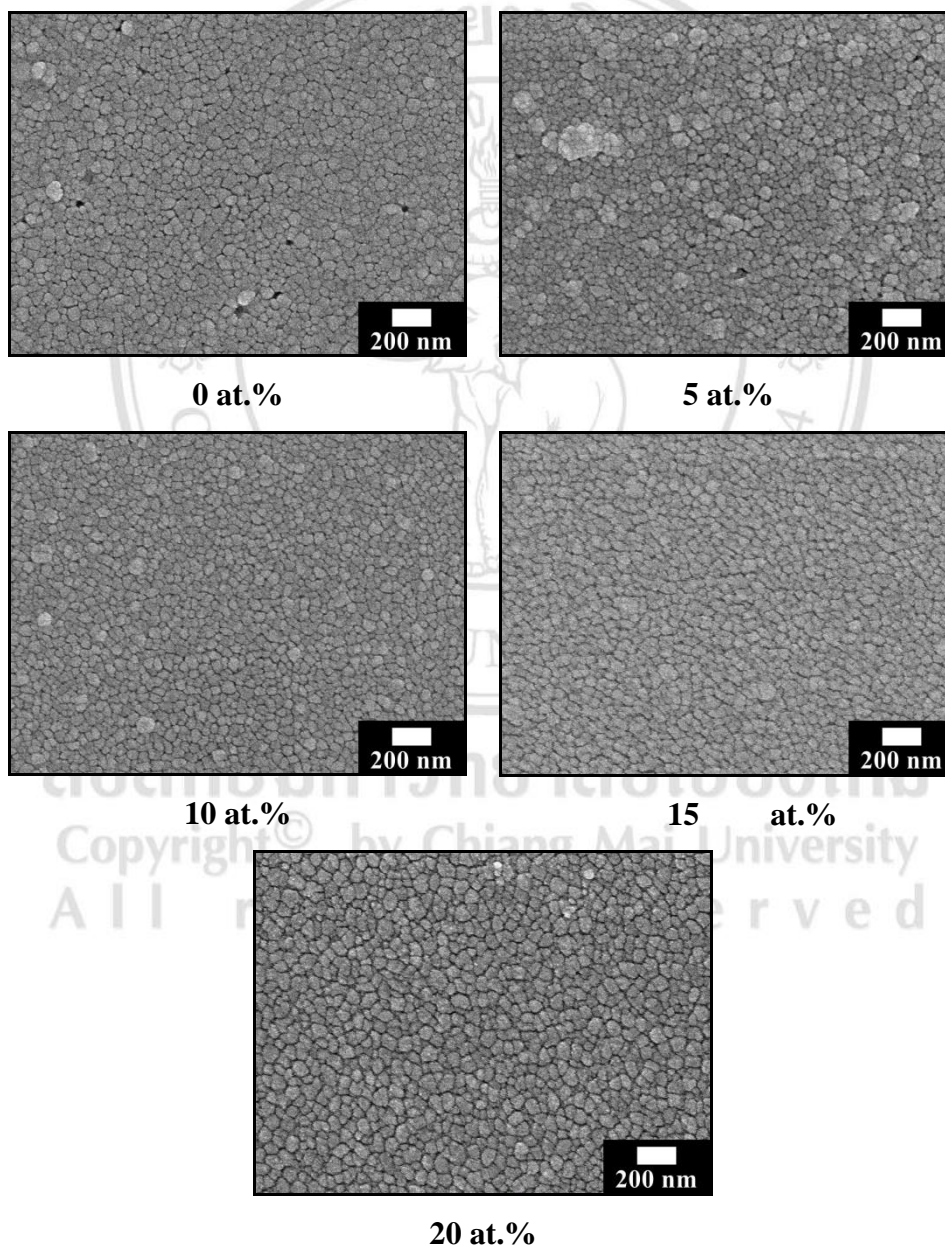


Figure 7.4 SEM images of Mg doped ZnO films with different Mg concentrations.

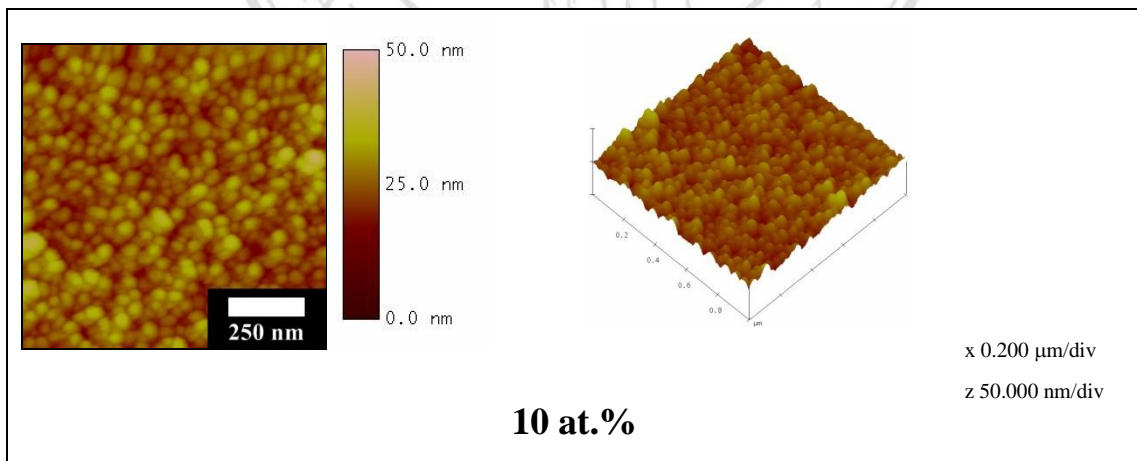
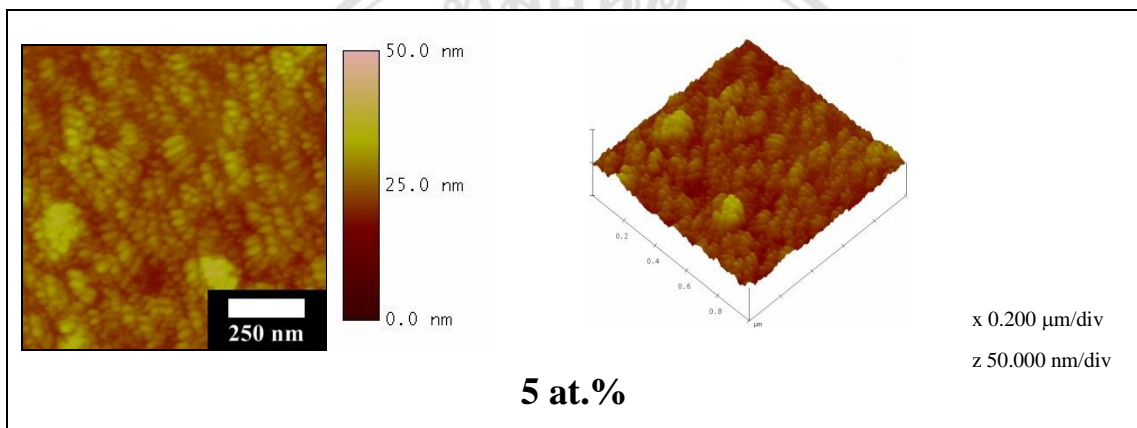
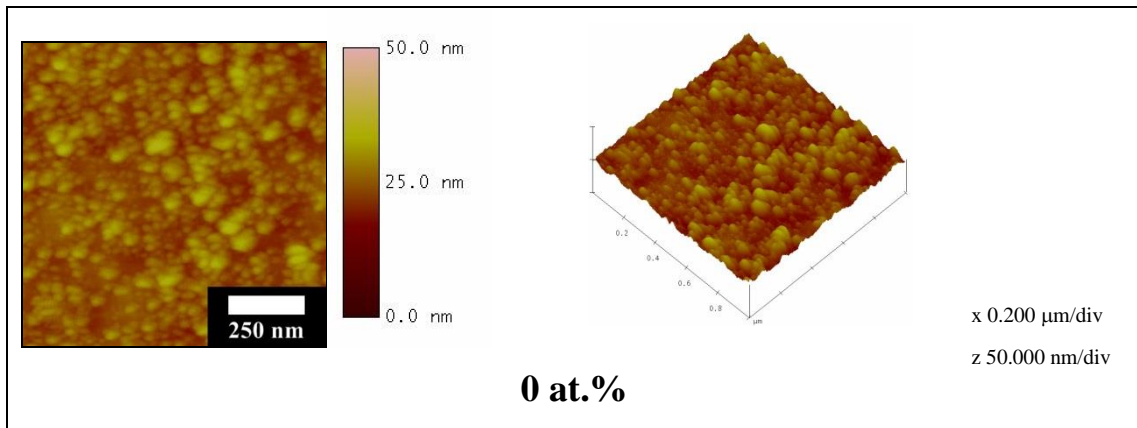


Figure 7.5 AFM images of Mg doped ZnO films with different Mg concentrations.

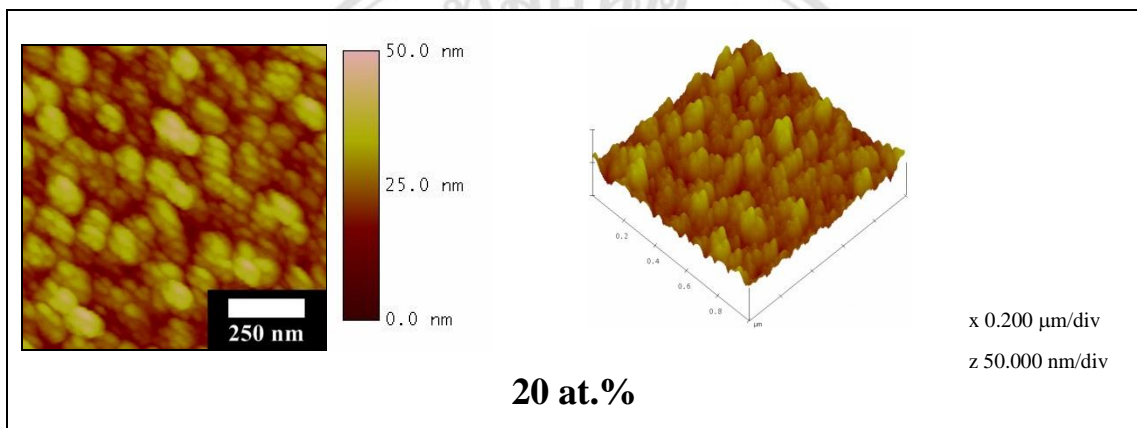
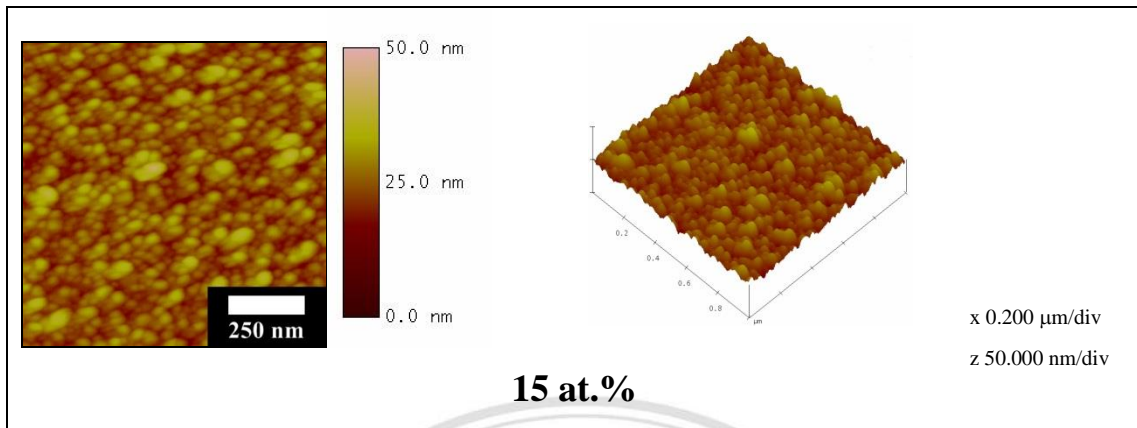


Figure 7.5 AFM images of Mg doped ZnO films with different Mg concentrations (continued).

The average grain size and surface roughness of films were obtained from these SEM and AFM images, respectively and presented in Figure 7.6. It was found that all films are homogeneous films with spherical shape and low surface roughness. The grain sizes of films do not change with addition Mg content, this result was opposite with the study in previous work (chapter 6). In addition, comparing the crystallite size of this work and previous work (chapter 6), it was found that the decreasing of $\text{Zn}(\text{CH}_3\text{OO})_2 \cdot 2\text{H}_2\text{O}$ concentration affected the decrease of crystallite size of films.

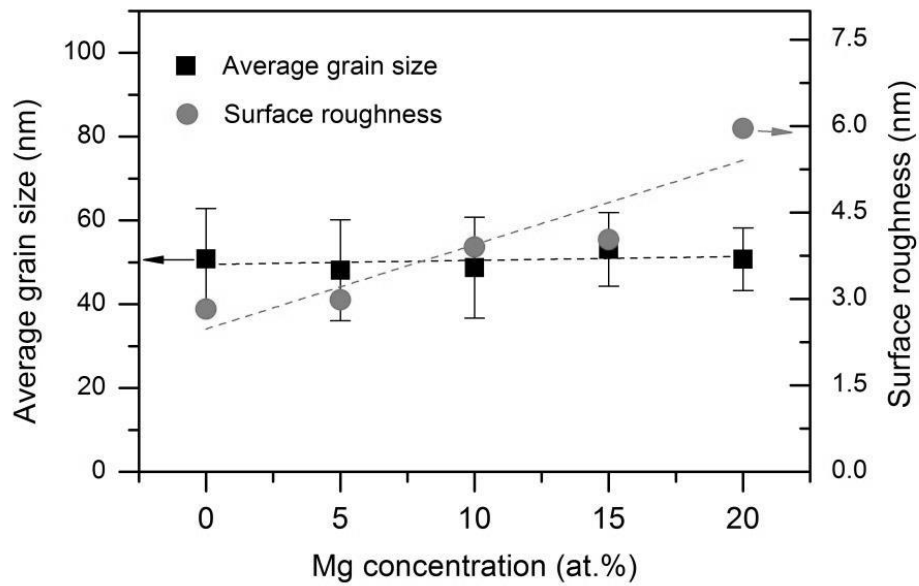


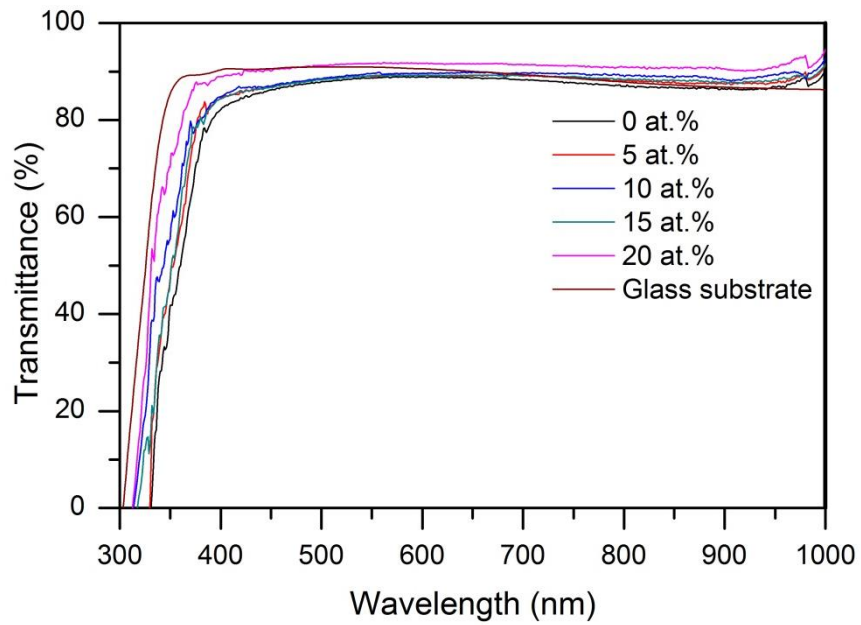
Figure 7.6 Average grain size and surface roughness of Mg doped ZnO films with different Mg concentrations.

7.2.4 Optical properties

The transmittance and absorbance spectra over the wavelength range 300-1000 nm of glass substrate and Mg doped ZnO films with different Mg concentration are shown in Figure 7.7. The transmittance and absorbance of undoped and Mg doped ZnO films are similar as about 90% and 0.01, respectively and all films showed a sharp ultraviolet cutoff. Moreover, a shift of the absorption edge occurred with added Mg content shifting to lower wavelengths (blue-shift).

The band gap was evaluated from this transmittance spectra and thickness (Table 7.2) using Tuac's relationship in equation 3.8. The $(\alpha h\nu)^2$ versus $h\nu$ plots of all films are shown in Figure 7.8 (a) The intercept of $(\alpha h\nu)^2$ on the x -axis gave the value of the direct band gap and the band gap of all films showed in Figure 7.8 (b). It was found that the band gap increased with increasing Mg content. This behavior was described by Huang et al. [61], Mg^{2+} induced a new defect after substituting Zn^{2+} because of the electronegativity and ionic radius difference of Zn (0.60 Å) and Mg (0.57

Å), which can be located at a higher Fermi level. This defect may create a higher Fermi level than for the initial ZnO films.



(a) Transmittance

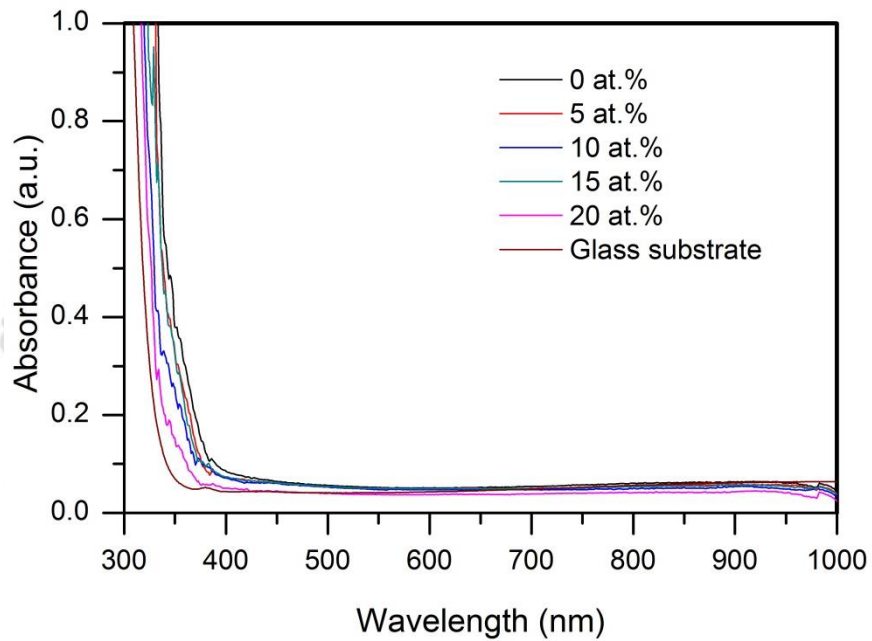
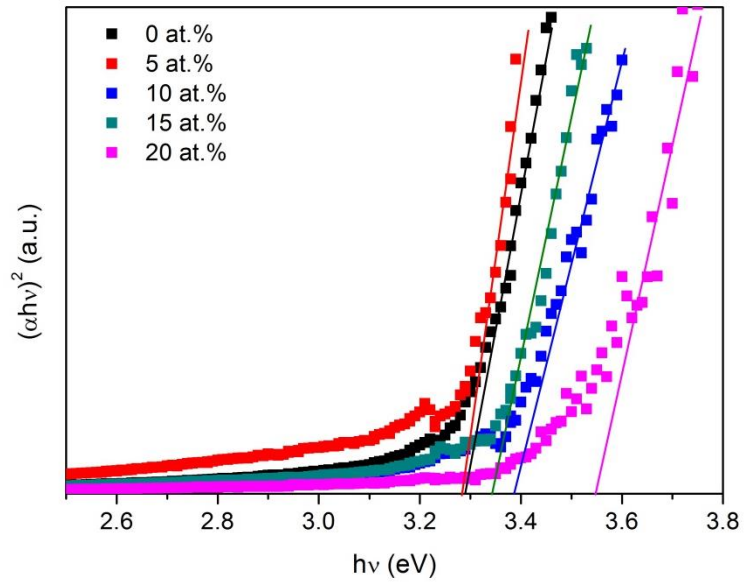
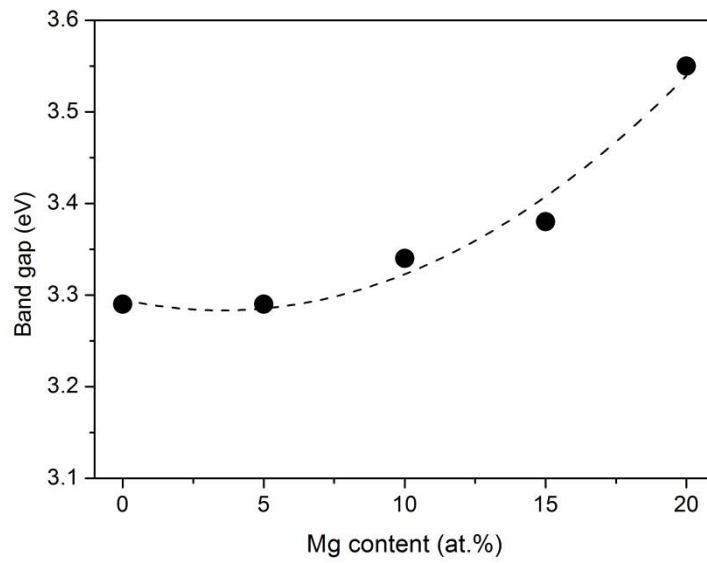


Figure 7.7 Transmittance (a) and absorbance (b) spectra of Mg doped ZnO films with different Mg concentrations.



(a) $(\alpha h\nu)^2$ versus $h\nu$ plots



(d) Band gap

Figure 7.8 The $(\alpha h\nu)^2$ versus $h\nu$ plots of Mg doped ZnO films with different Mg concentrations (a) and band gap (d) of these films.

7.2.5 Electrical property

The sheet resistance and the resistivity of of Mg doped ZnO films with different Mg concentration are shown in Figure 7.9. The resistivity is calculated from resistance and thickness of films by equation 3.10, the thickness was listed in Table 7.2.

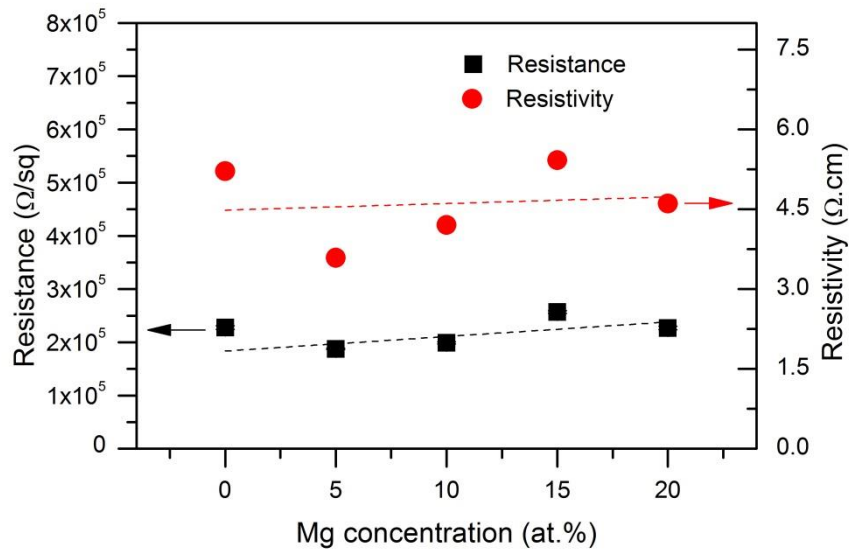


Figure 7.9 The sheet resistance and the resistivity of of Mg doped ZnO films with different Mg concentrations.

It was found that the similar resistivity values of undoped and Mg doped ZnO films. This similar behavior was observed in previous work (chapter 6). The similarity values were attributed to the partial substitution of Zn^{2+} ions by the same valence Mg^{2+} ions [58]. Hence, Mg^{2+} do not generated carriers in ZnO lattice [61].